Journal of
Composites Science

MDPI

Article

pH-Triggered Interfacial Interaction of Kaolinite/Chitosan Nanocomposites with Anionic Azo Dye

Shaikat Chandra Dey [1], Mokrema Moztahida [1,2], Mithun Sarker [1], Md. Ashaduzzaman [1] and Sayed Md. Shamsuddin [1,*]

[1] Department of Applied Chemistry and Chemical Engineering, Faculty of Engineering and Technology, University of Dhaka, Dhaka 1000, Bangladesh; shaikat@du.ac.bd (S.C.D.); moztahida@gmail.com (M.M.); mithun@du.ac.bd (M.S.); azaman01@du.ac.bd (M.A.)

[2] Department of Environmental Engineering, Kyungpook National University, Daegu 41566, Korea

* Correspondence: sdin@du.ac.bd; Tel.: +88-01-716-733-298

Received: 21 February 2019; Accepted: 28 March 2019; Published: 8 April 2019



Abstract: Advanced engineering of naturally occurring materials opens new doors in nanoscience and nanotechnology for the separation and/or removal of environmental hazards. Here, a series of nanocomposites containing kaolinite and chitosan varying in the range of 20 to 80% (w/w) kaolinite were used for the adsorptive removal of a reactive textile dye, Remazol Red, from an aqueous solution. Batch experiments were carried out to investigate the effects of pH, contact time, and initial dye concentration on the adsorption capacity. Nanocomposites containing 80% kaolinite (w/w) and 20% chitosan (w/w), i.e., $NK_{80}C_{20}$, showed an equilibrium adsorption capacity of 371.8 mg/g at pH 2.5, which was 5.2 times higher than that of commercial activated charcoal. Moreover, $NK_{80}C_{20}$ was regenerated instantly up to 99.9% at pH 10. Therefore, $NK_{80}C_{20}$ can be effectively utilized as a potential adsorbent for the separation of Remazol Red and homologous azo dyes from industrial effluents. We expect that the findings from this study will play a vital role in environmental research leading to advanced applications in water purification.

Keywords: nanocomposites; kaolinite; chitosan; Remazol Red; activated charcoal

1. Introduction

Nanocomposites (NCPs) offer several advantages and better performances over traditional composites since the interface and morphology of NCPs are totally different from those of traditional composite materials [1]. A large fraction of the polymer matrix is converted into an interface of different properties due to the smaller particle size and larger surface area of the dispersed phase, and also due to smaller inter-particle distances [2]. As a result, there is a substantial improvement in properties such as strength, flame retardancy, modulus, decrease in gas permeability, thermal stability, etc. [3]. These improved properties help NCPs find potential applications in various fields such as adsorbents, automotive industries, exterior step assists, tennis rackets, tennis balls, soccer balls, hockey sticks, tires, electrostatic dissipation, beverage containers, films, latex gloves, auto fuel systems, etc. [4]. Due to their environment-friendly and cost-effective nature, NCPs from waste and naturally occurring materials are gaining rapid interest for the remediation of hazardous pollutants [5–7].

Azo dyes, extensively used in textile industries, pose a great threat to both aquatic organisms and animals as they are toxic, carcinogenic, and mutagenic [8]. Due to their higher solubility in water, high molecular weight, and stability under the effects of light, heat, and oxidizing agents, it is very difficult to either degrade or remove these dyes from effluents with conventional wastewater treatment

methods [9]. Adsorptive removal is considered to be a highly efficient technique for the separation of these stubborn dyes from wastewater [10]. In this regard, biopolymer chitosan is an excellent choice because of its higher adsorption capacity for dyes. The enhanced adsorption capacity of chitosan has been attributed to the presence of hydroxyl (-OH) and amino (-NH_2) functional groups, which serve as reaction and coordination sites [11]. Since chitosan displays polycationic nature in acidic media due to the protonation of amino functional groups, it can strongly adsorb anionic azo dyes by the electrostatic force of attraction [12]. Remazol Red (RR) is an anionic reactive azo dye that contains a sulfonic acid group. Therefore, for the removal of RR from textile effluents, chitosan can be applied as a potential adsorbent, but it does have some limitations. Chitosan becomes soft in aqueous media due to its hydrophilicity and has a tendency to form a gel; it swells and floats in water. Furthermore, it has a low specific gravity and smaller surface area, weak mechanical properties, higher solubility in acidic media, etc. [13–15]. The formation of composites with chitosan has been considered an efficient pathway for overcoming these drawbacks [10].

Numerous researchers and their coworkers have performed several trials for developing efficient adsorbents from chitosan by incorporating different substrates such as sand [16], perlite [17], ceramic alumina [18], oil palm ash [19], calcium alginate [20], magnetite [21], polyurethane [22], cotton fiber [23], cellulose [24], polyvinyl alcohol [25], polyvinyl chloride [13], etc. However, the major focus has been on clay minerals [5–7,26–33]. Clay minerals are attractive immobilization/support materials for chitosan owing to their relatively large available surface areas [34]. Natural clay minerals are inexpensive since they are widely distributed in most continents of the world. Clay minerals can act as host materials with high sorption capacities due to their unique layered silicate structures [35]. Among various clay minerals, kaolinite is the most abundant phyllosilicate, which has a 1:1 type aluminosilicate structure consisting of SiO_2 (42.14 mol%), Al_2O_3 (15.61 mol%), and H_2O (42.25 mol%) [36,37]. The adsorption properties of kaolinite have been widely reported in the literature by many researchers [37–40].

To date, a few kaolinite/chitosan composite adsorbents have been reported in the literature [5–7]. Kanchana et al. reported a binary composite of nanochitosan/kaolin clay for the adsorption of Pb (II) [5]. Zhu et al. developed a ternary composite of chitosan/kaolin/nanosized γ-Fe_2O_3 for the adsorption of methyl orange [6]. Chen et al. prepared chitosan/coated kaolinite beads for the adsorption of Cu (II) [7]. In our previous study, we demonstrated a simple dropping technique for the fabrication of NCPs from kaolinite and chitosan [41]. However, to the best of our knowledge, there is no literature report on kaolinite/chitosan NCP adsorbents for the removal of RR. In this study, we report the adsorption performance of kaolinite/chitosan NCPs at various operating conditions of pH, contact time, and dye concentration. In addition, we clearly demonstrate the pH-controlled reversible interaction of RR with the adsorbent surface. Moreover, we investigated the probable mechanism for the variation of the adsorption performance of the NCPs with increasing kaolinite content. Because it offers several technological advantages in terms of facile fabrication, adsorption capacity, reusability, cost, and environment-friendly nature, the fabricated NCP is expected to find outstanding applications in the separation of azo dyes and similar hazardous pollutants from effluents of textile, food, leather, pharmaceutical, and other industries.

2. Materials and Methods

2.1. Materials

Kaolinite and waste prawn shells were collected from a local source in Bangladesh. Purified sodium hydroxide pellets and 35% hydrochloric acid (w/w) were supplied by Active Fine Chemicals Limited (Dhaka, Bangladesh). Acetic acid and ethanol were purchased from Merck KGaA (64271 Darmstadt, Germany). The selected azo dye (RR) was collected from a local textile industry in Bangladesh. All of the chemicals were used without further purification.

2.2. Methods

2.2.1. Preparation of NCPs

The NCPs were successfully prepared and characterized as reported in our recently published article [41]. The process we followed is briefly described here. Chitosan flakes were dissolved in 100 mL acetic acid (1 M) and kaolinite (acid activated) was then added to the chitosan solution. The resulting mixture was agitated by a sonicator for 30 min. The mixture was then sprayed dropwise into a neutralization solution of 15% NaOH (w/v) and 95% ethanol (v/v) in a volume ratio of 4:1. The formed composite beads were washed several times and dried in an oven at 60 °C for 10 h. The beads after drying were ground to reduce their size for the enhancement of adsorption capacity. Five different NCPs were prepared with different ratios of chitosan and kaolinite as shown in Table 1.

Table 1. Nanocomposites (NCPs) prepared from different proportions of chitosan and kaolinite.

NCP Code	% Chitosan (w/w)	% Kaolinite (w/w)	Chitosan:Kaolinite
$NK_{20}C_{80}$	80	20	4:1
$NK_{40}C_{60}$	60	40	3:2
$NK_{50}C_{50}$	50	50	1:1
$NK_{60}C_{40}$	40	60	2:3
$NK_{80}C_{20}$	20	80	1:4

2.2.2. Thermogravimetric Analysis (TGA)

Thermal stability of the NCPs was examined by a thermogravimetric analyzer (TGA-50, Shimadzu Corporation, Kyoto, Japan) with an alumina cell under a nitrogen atmosphere at the flow rate of 10 mL/min (for both balance and sample) and at the heating rate of 10 °C/min. The samples were heated from 25 °C to 1000 °C. From TGA data, the loading of chitosan in mmol per mol of kaolinite was calculated.

2.2.3. Adsorption of RR

Twenty (20) milliliters of RR solution with different concentrations (from 60 to 100 ppm) were added to Erlenmeyer flasks with air-tight stoppers. Five (5) milligrams of each type of NCP was used throughout the adsorption study. For adjusting the pH of the solutions, 0.1 M NaOH and 0.1 M HCl were employed. The flasks were shaken at room temperature (25 °C) by a shaker at 150 rpm until the equilibrium point was reached. An ultraviolet (UV)-Vis spectrophotometer (UV-2100PC HumanLab Instrument Co., Suwon-city, Korea) was used to determine the concentration of RR in the solution by measuring the absorbance at 518 nm (Figure S1). The equilibrium adsorption capacity (q_e) was calculated according to the following formula:

$$q_e = \frac{(C_o - C_e)V}{m}$$

where C_o is the initial concentration of RR (ppm), C_e is the equilibrium concentration of RR (ppm), m is the weight of the adsorbent used for the adsorption studies (g), and V is the volume of RR solution taken (L).

2.2.4. Desorption of RR

The regeneration of an adsorbent is very important for its practical application. After adsorption, the dye-loaded adsorbents were subjected to alkaline media of pH 8.0, 9.0, and 10.0 in order to investigate their regeneration efficiency.

3. Results and Discussions

3.1. Effect of Operating Conditions

Various parameters, e.g., surface charge of an adsorbent, degree of ionization, structural changes of dye molecules, dissociation of functional groups on its active sites, etc., are strongly affected by the pH of the solution [42]. We closely monitored the effects of pH, contact time, and initial RR concentration on the adsorption capacity of NCPs.

3.1.1. Effect of pH

In our previous study, we demonstrated the influence of pH on the adsorption of RR by chitosan (Figure 1a) [43]. Chitosan showed an adsorption capacity of 313.4 mg/g at pH 3.0. In acidic media, there was a strong electrostatic force of attraction between the anionic RR molecules and chitosan due to the protonation of the amino functional groups on the surface of chitosan. The highest adsorption capacity of chitosan at pH 3.0 might be attributed to the maximum protonation of the amino functional groups at pH 3.0. The decrease in adsorption capacity at a pH below 3 might occur due to the dissolution of chitosan. When the pH of the solution was increased above 3, the adsorption capacity also decreased because of the lower degree of protonation of amino functional groups. Chitosan exhibited a very low adsorption capacity at a pH above 7 because the amino functional groups of chitosan no longer remained protonated in alkaline media.

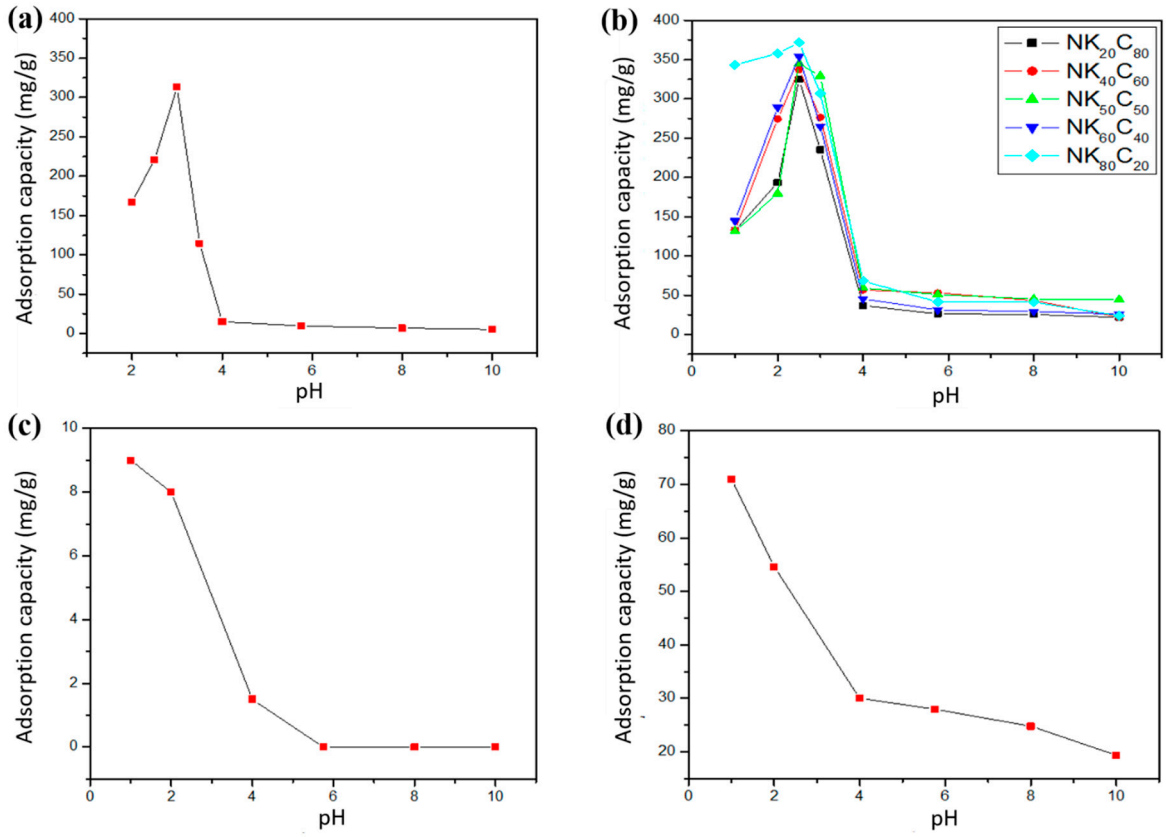


Figure 1. Effect of pH on the adsorption capacity of (**a**) chitosan, (**b**) nanocomposites (NCPs), (**c**) kaolinite, and (**d**) activated charcoal.

All of the NCPs showed a higher adsorption capacity than chitosan and kaolinite as presented in Figure 1b. However, the adsorption behavior was similar to chitosan. There was only one exception which was that the maximum adsorption occurred at pH 2.5 for the NCPs, not at pH 3.0. Ngah et al. also reported the maximum adsorption capacity of a crosslinked chitosan-coated bentonite bead for anionic tartrazine at pH 2.5 [44]. The similarity between the two studies at a particular pH strongly supports that 2.5 could be the most suitable pH for the adsorption of anionic dye molecules by chitosan/clay composites. The pH stability of chitosan was improved due to the attachment of chitosan on the surface of kaolinite in the formation of the composite, which resisted the dissolution of chitosan up to pH 2.5. The adsorption behavior of $NK_{80}C_{20}$ below pH 2.5 was totally different from others, as explained later.

In the case of kaolinite, as depicted in Figure 1c, there was a progressive increase in the adsorption capacity as the pH of solution decreased below 6. The maximum adsorption capacity of 9 mg/g was observed at pH 1.0. In acidic media, protons were available which were responsible for the electrostatic attraction between the negatively charged RR molecules and the kaolinite surface. With the gradual decrease in the pH of the solution, there was a progressive increase in the availability of protons resulting in the enhanced adsorption of RR molecules. With an increase in the pH of the solution, there was a relative decrease in the positive charge on the surface and an increase in the negative charge. Adsorption of anionic dyes was not favored on the negatively charged kaolinite surface due to electrostatic repulsion. Also, in alkaline media, there was competition between the hydroxyl ions and the dye anions for the adsorbent [45].

The formation of NCPs not only eliminated the crystallinity of chitosan but also caused an increase in specific gravity. Chitosan is a semi-crystalline polymer and, as a result, the penetration of dye molecules through the crystalline region is very difficult. Prior to composite formation, chitosan was dissolved in acetic acid, which caused the loss of crystallinity. Moreover, NCPs possessed higher surface area than the flaky chitosan due to the smaller particle size. All of these factors contributed to the higher adsorption capacity of NCPs as compared to chitosan.

The adsorption performance of the NCPs was compared with the commercial activated charcoal. Activated charcoal showed an adsorption capacity of only 71 mg/g for RR at pH 1.0, as illustrated in Figure 1d. This capacity was very low compared to chitosan and $NK_{80}C_{20}$. The comparison strongly supports the notion that kaolinite/chitosan NCPs have huge potential to be industrially used as adsorbents for anionic azo dyes.

3.1.2. Effect of Contact Time

The fundamental basis of adsorption kinetics is the effect of contact time on the adsorption capacity [46].

Figure 2a,b depict the effect of contact time on the adsorption capacity of chitosan and $NK_{80}C_{20}$ for RR.

In the case of chitosan, as illustrated in Figure 2a, the rate of adsorption was very rapid up to the first 20 min and then the rate was very slow. The equilibrium was reached after 30 min. In the case of $NK_{80}C_{20}$, as shown in Figure 2b, the rate of adsorption increased rapidly during the first 10 min, then increased slowly and after 15 min reached equilibrium. The higher initial rate of adsorption is attributed to the higher number of vacant active sites on the surface of the adsorbent. Dye molecules gradually cover these active sites, but near the equilibrium it is difficult for the dye molecules to occupy the remaining active sites, probably due to the slow pore diffusion [47]. Contact times of 30 min and 15 min were selected for chitosan and $NK_{80}C_{20}$, respectively, for further study.

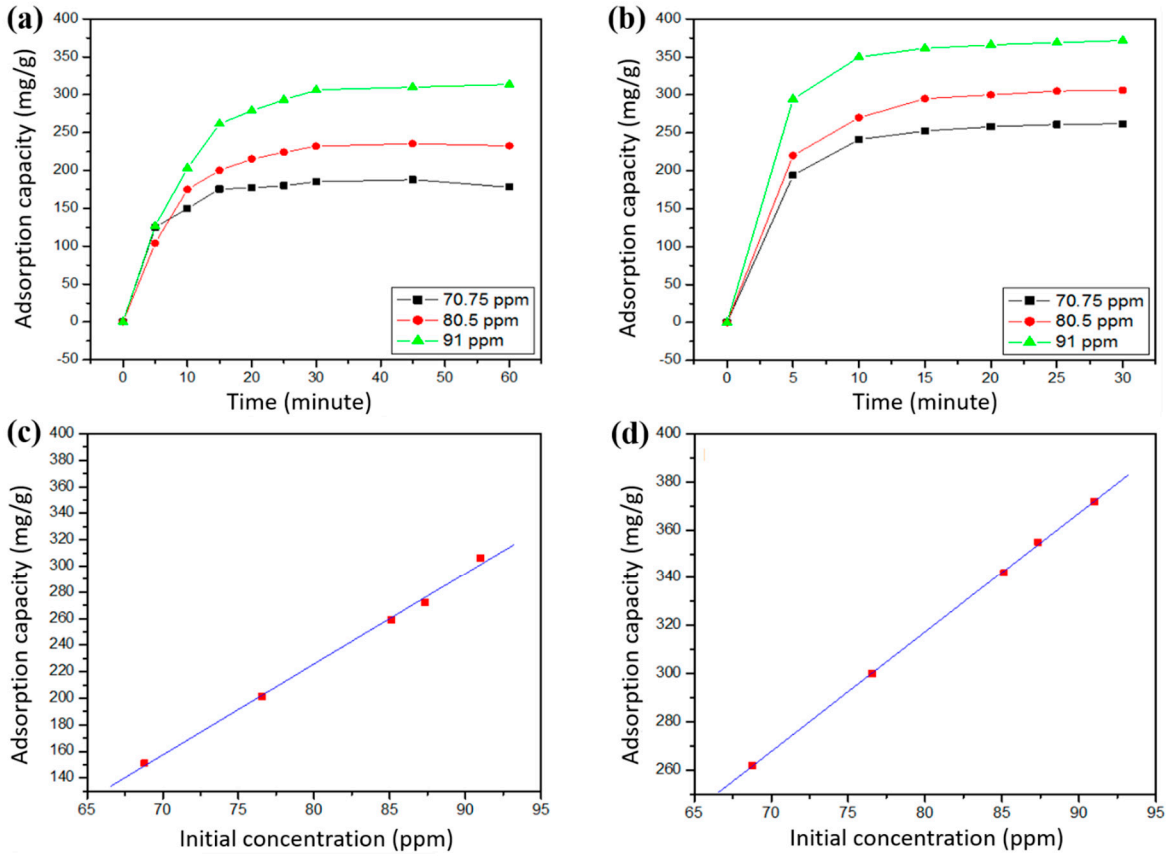


Figure 2. Effect of contact time on the adsorption capacity of (**a**) chitosan and (**b**) $NK_{80}C_{20}$; effect of the initial concentration of Remazol Red (RR) on the adsorption capacity of (**c**) chitosan and (**d**) $NK_{80}C_{20}$.

3.1.3. Effect of Initial RR Concentration

The adsorption capacity of both chitosan and $NK_{80}C_{20}$ was influenced by the initial RR concentration. As shown in Figure 2c,d, it was observed that the adsorption capacity of both chitosan and $NK_{80}C_{20}$ increased with increasing the initial concentration of RR. During the adsorption process, dye molecules are diffused from the bulk of the solution to the adsorbent surface. The driving force for this mass transfer process is the concentration gradient between the bulk of the solution and the adsorbent surface [48]. With an increase in the initial RR concentration, the concentration gradient increased, resulting in the enhanced diffusion of RR molecules. As a result, the rate of adsorption of RR on both chitosan and $NK_{80}C_{20}$ increased with increasing the initial concentration of RR.

3.2. Mechanistic View of Adsorption Performance

As shown in Figure 3a, the NCPs showed a progressive increase in adsorption capacity with the increase in kaolinite content. Among the NCPs, the lowest adsorption capacity of 325 mg/g found was for $NK_{20}C_{80}$ and the highest adsorption capacity of 371.8 mg/g found was for $NK_{80}C_{20}$. Here, we propose a mechanism for the progressive increase in adsorption capacity with the gradual increase in kaolinite content, which is illustrated in Figure 3b.

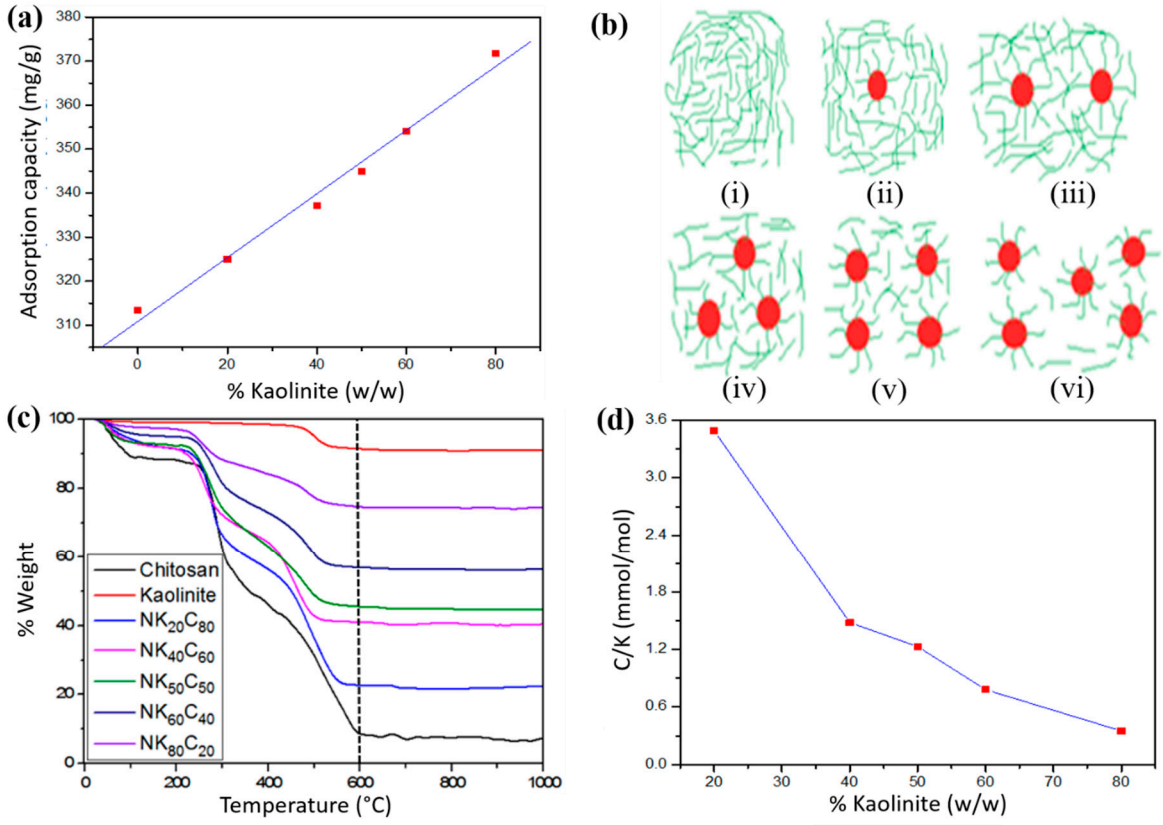


Figure 3. (**a**) Effect of kaolinite content on the adsorption capacity of NCPs; (**b**) proposed interaction between kaolinite and chitosan: (**i**) chitosan, (**ii**) $NK_{20}C_{80}$, (**iii**) $NK_{40}C_{60}$, (**iv**) $NK_{50}C_{50}$, (**v**) $NK_{60}C_{40}$, and (**vi**) $NK_{80}C_{20}$; (**c**) thermogravimetric analysis (TGA) thermograms; and (**d**) effect of kaolinite content on the loading of chitosan on kaolinite.

Due to low specific gravity, soft and flexible chitosan swelled and floated in water. The polymer could not move uniformly throughout the dye solution and its effective contact with the dye molecules was low. Therefore, it showed low adsorption capacity. With the incorporation of kaolinite, the macromolecule electrostatically attached itself to the heavier kaolinite nanoparticles. The specific gravity of the macromolecules was increased due to their self-assembly on the negatively charged kaolinite surface. The movement of NCPs was more uniform throughout the dye solution as compared to the movement of chitosan alone. In these NCP systems, the surface-attached chitosan found more scope for effective contact with the dye molecules. The number of surface-attached chitosan increased gradually with increasing the kaolinite content. In this study, the porous structure of the chitosan-immobilized NCPs played a vital role in adsorption. In the case of $NK_{20}C_{80}$, chitosan might form densely packed multilayers on the kaolinite surface. This hard shell showed an adsorption behavior similar to that of chitosan. In the case of $NK_{80}C_{20}$, kaolinite might be partially covered, i.e., chitosan might form less densely packed thin layers on the kaolinite surface. This soft shell showed the highest adsorption behavior. The charge distribution on the surface at this condition might create a suitable environment for the NCP, facilitating the interaction tendency towards dye uniformly. Because it exhibited the most effective surface attachment, $NK_{80}C_{20}$ showed the highest adsorption capacity at pH 2.5 and the highest resistance to dissolution below pH 2.5 as compared to the other NCPs.

3.3. Thermogravimetric Analysis (TGA)

Some useful information was derived from the TGA thermograms as illustrated in Figure 3c. From the thermograms, it was observed that chitosan decomposed at 600 °C, whereas no

decomposition of kaolinite occurred at this temperature. The content of thermally stable kaolinite controlled the decomposition pattern of the NCPs. Based on the weight loss of the NCPs at 600 °C, we calculated the loading of chitosan in mmol per mol of kaolinite using their respective molecular weights. As demonstrated in Figure 3d, the highest amount of chitosan in mmol was loaded per mol of kaolinite in the case of $NK_{20}C_{80}$, whereas the least amount of chitosan loading was calculated for $NK_{80}C_{20}$.

3.4. Surface Charge Calculation

The surface charge of an adsorbent plays the determining role in the adsorption process. Therefore, it is very important to quantify the charge distribution on the surface of an adsorbent. Since $NK_{80}C_{20}$ showed the highest adsorption capacity, we calculated the surface charge per gram of $NK_{80}C_{20}$. The value for $NK_{80}C_{20}$ was calculated to be 109 C. The protonation of amino functional groups at pH 2.5 was responsible for the presence of a positive charge on the surface of the $NK_{80}C_{20}$. This quantity of positive charge on the surface must be balanced by an equivalent quantity of negative charge on the adsorbed dye molecules. The adsorption capacity for $NK_{80}C_{20}$ was 371.8 mg/g, i.e., 371.8 mg dye must carry an equivalent quantity of negative charge to balance the 109 C positive charge. The estimated charge on 371.8 mg of RR was 147 C. RR is an anionic azo dye and the highest adsorption capacity was found at pH 2.5. Therefore, at this strong acidic condition the additional 38 C negative charge on RR might be balanced by the protonated azo functional groups [49].

3.5. Demonstration of a Reversible Interaction

Since acidic media were preferable for the adsorption of RR by both chitosan and $NK_{80}C_{20}$, we employed alkaline media for their regeneration. Alkaline pH played a vital role in the regeneration of these two adsorbents because there was an immediate desorption of dye molecules from both chitosan and $NK_{80}C_{20}$ (Figure 4a). The pH-controlled reversible interaction between NCPs and RR in the aqueous phase is schematically illustrated in Figure 4b.

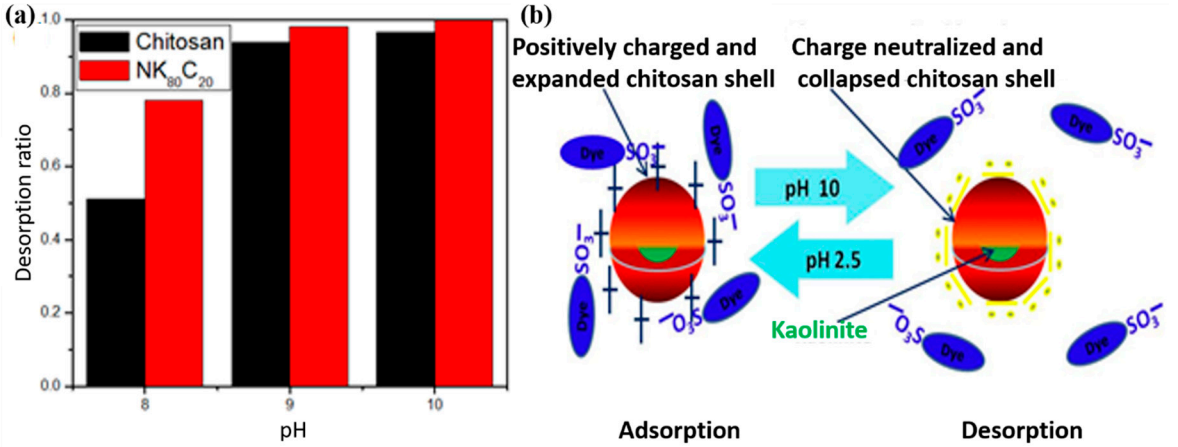


Figure 4. (**a**) Bar diagram of desorption ratio vs. pH and (**b**) schematic illustration for the adsorption–desorption mechanism of RR.

With the gradual increase in pH of the media, there was a progressive increase in the desorption of RR from both chitosan and $NK_{80}C_{20}$. As depicted in Figure 4b, the dye molecules were trapped on the NCP surface at pH 2.5 but at pH 10, the captured dye molecules were liberated from the surface. Therefore, the adsorbent was regenerated and was ready to be used again. From this schematic representation, it can be concluded that the interfacial interaction of $NK_{80}C_{20}$ with RR was reversible, and was completely controlled by the pH of the medium. This interfacial interaction was further confirmed by recording the FTIR spectrum of dye-loaded $NK_{80}C_{20}$ (Figure S2). Chitosan and $NK_{80}C_{20}$ showed the highest desorption ratios of 0.967 and 0.999, respectively, at pH 10.0. The dye molecules

might be trapped inside the spiral polymeric chains of chitosan. However, in the case of $NK_{80}C_{20}$, the spiral chains could be more disentangled. This factor might contribute to the higher desorption of RR from $NK_{80}C_{20}$ than from chitosan.

3.6. Comparison of Adsorption Performance

According to previously reported literature, treated sawdust showed an adsorption capacity of only 8.0 mg/g for RR at pH 2.0 after a very long time of 12 h [50]. In our previous study, chitosan showed an adsorption capacity of 313.4 mg/g for RR at pH 3.0 after 30 min [43]. However, in this present study, we found that the fabrication of kaolinite/chitosan NCPs enhanced the adsorption capacity of chitosan for RR. Moreover, there was a successive increase in the adsorption capacity of the NCPs with the gradual increase in kaolinite content, due to the progressive formation of self-assembly. Out of the five NCPs, $NK_{80}C_{20}$ contained only 20% (w/w) chitosan and 80% (w/w) kaolinite. Kaolinite is a naturally occurring and cheap raw material, whereas chitosan needs to be prepared from waste prawn shells through some expensive chemical steps. Therefore, the NCP prepared with the least amount of chitosan and the highest amount of kaolinite should be the cheapest one. Out of the five NCPs utilized in this study, $NK_{80}C_{20}$ was the most cost-effective composite. $NK_{80}C_{20}$ also showed the highest adsorption capacity of 371.8 mg/g within only 15 min and had 99.9% instant regeneration. We also employed the widely used adsorbent, i.e., activated charcoal for the adsorption of RR. However, it showed an adsorption capacity of only 71 mg/g for RR at pH 1.0. Therefore, from the discussion above, it can be said that $NK_{80}C_{20}$ is a much more effective adsorbent for RR as compared to other adsorbents reported in literature.

The potential differences between chitosan and $NK_{80}C_{20}$, as found in this study, are summarized in Table 2 and Figure S3 clearly distinguishes their adsorption performance.

Table 2. Comparison of adsorption performance between chitosan and $NK_{80}C_{20}$.

Parameters	Chitosan	$NK_{80}C_{20}$
Adsorption capacity, mg/g	313.4 (% Error: 6)	371.8 (% Error: 5)
Optimized pH	3.0	2.5
% Removal of RR	84.1	99.6
Equilibrium time, min	30	15
Desorption ratio	0.967	0.999

4. Conclusions

Hazardous pollutants have severe negative environmental impacts. In order to defend nature against such detrimental impacts, nanoscience and nanotechnology can play a pivotal role. In this study, we report kaolinite/chitosan NCPs as a potential remedy for water pollution by RR. We closely observed that the fabrication of NCPs improved the pH stability and adsorption capacity of chitosan. All of the NCPs exhibited a higher adsorption capacity than kaolinite, chitosan, and activated charcoal. The NCPs showed a successive increase in the adsorption capacity with a gradual increase in kaolinite content, due to the progressive formation of self-assembly. The pH-controlled interaction of NCPs with RR has been clearly demonstrated in this report. Self-assembly of the majority of the polymeric chains on the kaolinite's surface contributed to the maximum capture of dye molecules on $NK_{80}C_{20}$. The higher adsorption capacity, quick and higher regeneration efficiency, and cost-effective nature of $NK_{80}C_{20}$ indicate that for the removal of RR and similar pollutants from industrial effluents, $NK_{80}C_{20}$ can be effectively utilized as a potential adsorbent.

Supplementary Materials: The following are available online at http://www.mdpi.com/2504-477X/3/2/39/s1, Figure S1: Visible spectra for aqueous solutions of RR; Figure S2: FTIR spectrum of (**a**) RR, (**b**) $NK_{80}C_{20}$, and (**c**) RR-loaded $NK_{80}C_{20}$; Figure S3: Image of (**a**) RR solution before adsorption, (**b**) RR solution after adsorption by chitosan, and (**c**) RR solution after adsorption by $NK_{80}C_{20}$.

Author Contributions: Conceptualization, S.M.S. and M.A.; Data curation, S.C.D.; Formal analysis, S.C.D., M.M. and M.S.; Funding acquisition, S.M.S.; Investigation, S.C.D.; Methodology, S.C.D., M.A. and S.M.S.; Project administration, S.M.S.; Resources, S.M.S.; Supervision, S.M.S. and M.A.; Visualization, S.C.D.; Writing—original draft, S.C.D.; Writing—review and editing, S.C.D., M.M., M.S., M.A. and S.M.S.

Funding: This research was funded by the Ministry of Science and Technology, Bangladesh (grant no. 39.0009.002.01.00.053. 2014-2015/EAS-243/668).

Acknowledgments: The authors are grateful to the Center for Advanced Research in Sciences (CARS) at University of Dhaka, Bangladesh for providing the TGA facility.

Conflicts of Interest: The authors declare no conflict of interest.

References

1. Bhattacharya, M.; Chen, B. Polymer Nanocomposites—A Comparison between Carbon Nanotubes, Graphene, and Clay as Nanofillers. *Materials* **2016**, *9*, 262. [CrossRef]
2. Bréchet, Y.; Cavaillé, J.Y.; Chabert, E.; Chazeau, L.; Dendievel, R.; Flandin, L.; Gauthier, C. Polymer based nanocomposites: Effect of filler-filler and filler-matrix interactions. *Adv. Eng. Mater.* **2001**, *3*, 571–577. [CrossRef]
3. Mittal, V. Polymer Layered Silicate Nanocomposites: A Review. *Materials* **2009**, *2*, 992–1057. [CrossRef]
4. Paul, D.; Robeson, L. Polymer nanotechnology: Nanocomposites. *Polymer* **2008**, *49*, 3187–3204. [CrossRef]
5. Kanchana, V.; Gomathi, T.; Geetha, V.; Sudha, P. Adsorption analysis of Pb (II) by nanocomposites of chitosan with methyl cellulose and clay. *Der Pharm. Lett.* **2012**, *4*, 1071–1079.
6. Zhu, H.-Y.; Jiang, R.; Xiao, L. Adsorption of an anionic azo dye by chitosan/kaolin/γ-Fe_2O_3 composites. *Appl. Clay Sci.* **2010**, *48*, 522–526. [CrossRef]
7. Chen, I.P.; Kan, C.C.; Futalan, C.M.; Calagui, M.J.C.; Lin, S.S.; Tsai, W.C.; Wan, M.W. Batch and fixed bed studies: Removal of copper (II) using chitosan-coated kaolinite beads from aqueous solution. *Sustain. Environ. Res.* **2015**, *25*, 73–81.
8. Puvaneswari, N.; Muthukrishnan, J.; Gunasekaran, P. Toxicity assessment and microbial degradation of azo dyes. *J. Exp. Boil.* **2006**, *44*, 618–626.
9. Joshi, M.; Bansal, R.; Purwar, R. Colour removal from textile effluents. *Indian J. Fibre Text. Res.* **2004**, *29*, 239–259.
10. Teong, L.; Hanafiah, M.A.K.M.; Ngah, W.W. Adsorption of dyes and heavy metal ions by chitosan composites: A review. *Carbohydr. Polym.* **2011**, *83*, 1446–1456.
11. Wu, F.-C.; Tseng, R.-L.; Juang, R.-S. Enhanced abilities of highly swollen chitosan beads for color removal and tyrosinase immobilization. *J. Hazard. Mater.* **2001**, *81*, 167–177. [CrossRef]
12. Kumar, M.N.R. A review of chitin and chitosan applications. *React. Funct. Polym.* **2000**, *46*, 1–27. [CrossRef]
13. Popuri, S.R.; Vijaya, Y.; Boddu, V.M.; Abburi, K. Adsorptive removal of copper and nickel ions from water using chitosan coated PVC beads. *Bioresour. Technol.* **2009**, *100*, 194–199. [CrossRef]
14. Hasan, S.; Ghosh, T.K.; Viswanath, D.S.; Boddu, V.M. Dispersion of chitosan on perlite for enhancement of copper(II) adsorption capacity. *J. Hazard. Mater.* **2008**, *152*, 826–837. [CrossRef]
15. Chiou, M.-S.; Li, H.-Y. Equilibrium and kinetic modeling of adsorption of reactive dye on cross-linked chitosan beads. *J. Hazard. Mater.* **2002**, *93*, 233–248. [CrossRef]
16. Wan, M.-W.; Kan, C.-C.; Rogel, B.D.; Dalida, M.L.P. Adsorption of copper (II) and lead (II) ions from aqueous solution on chitosan-coated sand. *Carbohydr. Polym.* **2010**, *80*, 891–899. [CrossRef]
17. Kalyani, S.; Priya, J.A.; Rao, P.S.; Krishnaiah, A. Removal of Copper and Nickel from Aqueous Solutions Using Chitosan Coated on Perlite as Biosorbent. *Sep. Sci. Technol.* **2005**, *40*, 1483–1495. [CrossRef]
18. Boddu, V.M.; Abburi, K.; Randolph, A.J.; Smith, E.D. Removal of copper (II) and nickel (II) ions from aqueous solutions by a composite chitosan biosorbent. *Sep. Sci. Technol.* **2008**, *43*, 1365–1381. [CrossRef]
19. Hasan, M.; Ahmad, A.L.; Hameed, B. Adsorption of reactive dye onto cross-linked chitosan/oil palm ash composite beads. *Chem. Eng. J.* **2008**, *136*, 164–172. [CrossRef]
20. Vijaya, Y.; Popuri, S.R.; Boddu, V.M.; Krishnaiah, A. Modified chitosan and calcium alginate biopolymer sorbents for removal of nickel (II) through adsorption. *Carbohydr. Polym.* **2008**, *72*, 261–271. [CrossRef]
21. Tran, H.V.; Tran, L.D.; Nguyen, T.N. Preparation of chitosan/magnetite composite beads and their application for removal of Pb(II) and Ni(II) from aqueous solution. *Mater. Sci. Eng. C* **2010**, *30*, 304–310. [CrossRef]

22. Lee, H.C.; Jeong, Y.G.; Gil Min, B.; Lyoo, W.S.; Lee, S.C. Preparation and acid dye adsorption behavior of polyurethane/chitosan composite foams. *Fibers Polym.* **2009**, *10*, 636–642. [CrossRef]
23. Zhang, G.; Qu, R.; Sun, C.; Ji, C.; Chen, H.; Wang, C.; Niu, Y. Adsorption for metal ions of chitosan coated cotton fiber. *J. Appl. Polym. Sci.* **2008**, *110*, 2321–2327. [CrossRef]
24. Sun, X.; Peng, B.; Ji, Y.; Chen, J.; Li, D. Chitosan(chitin)/cellulose composite biosorbents prepared using ionic liquid for heavy metal ions adsorption. *AIChE J.* **2009**, *55*, 2062–2069. [CrossRef]
25. Kumar, M.; Tripathi, B.P.; Shahi, V.K. Crosslinked chitosan/polyvinyl alcohol blend beads for removal and recovery of Cd(II) from wastewater. *J. Hazard. Mater.* **2009**, *172*, 1041–1048. [CrossRef]
26. Rekik, S.B.; Gassara, S.; Bouaziz, J.; Deratani, A.; Baklouti, S. Development and characterization of porous membranes based on kaolin/chitosan composite. *Appl. Clay Sci.* **2017**, *143*, 1–9. [CrossRef]
27. Rekik, S.B.; Gassara, S.; Bouaziz, J.; Deratani, A.; Baklouti, S. Enhancing hydrophilicity and permeation flux of chitosan/kaolin composite membranes by using polyethylene glycol as porogen. *Appl. Clay Sci.* **2019**, *168*, 312–323. [CrossRef]
28. Bertolino, V.; Cavallaro, G.; Lazzara, G.; Milioto, S.; Parisi, F. Halloysite nanotubes sandwiched between chitosan layers: Novel bionanocomposites with multilayer structures. *New J. Chem.* **2018**, *42*, 8384–8390. [CrossRef]
29. Souza, V.G.L.; Pires, J.R.A.; Vieira, É.; Coelhoso, I.M.; Duarte, M.P.; Fernando, A.L. Shelf Life Assessment of Fresh Poultry Meat Packaged in Novel Bionanocomposite of Chitosan/Montmorillonite Incorporated with Ginger Essential Oil. *Coatings* **2018**, *8*, 177. [CrossRef]
30. Bertolino, V.; Cavallaro, G.; Milioto, S.; Parisi, F.; Lazzara, G. Thermal Properties of Multilayer Nanocomposites Based on Halloysite Nanotubes and Biopolymers. *J. Compos. Sci.* **2018**, *2*, 41. [CrossRef]
31. dos Santos, B.F.F.; Maciel, M.A.; Tavares, A.A.; de Araújo Fernandes, C.Q.B.; de Sousa, W.J.B.; Lia Fook, M.V.; Leite, I.F.; De Lima Silva, S.M. Synthesis and preparation of chitosan/clay microspheres: Effect of process parameters and clay type. *Materials* **2018**, *11*, 2523. [CrossRef]
32. Ben Dhieb, F.; Dil, E.J.; Tabatabaei, S.H.; Mighri, F.; Ajji, A. Effect of nanoclay orientation on oxygen barrier properties of LbL nanocomposite coated films. *RSC Adv.* **2019**, *9*, 1632–1641. [CrossRef]
33. Li, X.; Li, Y.-C.; Chen, M.-J.; Shi, Q.; Sun, R.; Wang, X. Chitosan/rectorite nanocomposite with injectable functionality for skin hemostasis. *J. Mater. Chem. B* **2018**, *6*, 6544–6549. [CrossRef]
34. Wu, P.; Wu, W.; Li, S.; Xing, N.; Zhu, N.; Li, P.; Wu, J.; Yang, C.; Dang, Z. Removal of Cd^{2+} from aqueous solution by adsorption using Fe-montmorillonite. *J. Hazard. Mater.* **2009**, *169*, 824–830. [CrossRef]
35. Monvisade, P.; Siriphannon, P. Chitosan intercalated montmorillonite: Preparation, characterization and cationic dye adsorption. *Appl. Clay Sci.* **2009**, *42*, 427–431. [CrossRef]
36. Alkan, M.; Kalay, B.; Doğan, M.; Demirbaş, Ö. Removal of copper ions from aqueous solutions by kaolinite and batch design. *J. Hazard. Mater.* **2008**, *153*, 867–876. [CrossRef]
37. Nandi, B.; Goswami, A.; Purkait, M. Adsorption characteristics of brilliant green dye on kaolin. *J. Hazard. Mater.* **2009**, *161*, 387–395. [CrossRef]
38. Zou, W.; Zhao, J.; Sun, C. Adsorption of Anionic Polyacrylamide onto Coal and Kaolinite Calculated from the Extended DLVO Theory Using the van Oss-Chaudhury-Good Theory. *Polymers* **2018**, *10*, 113. [CrossRef]
39. Zhang, J.; Lu, S.; Li, J.; Xue, H.; Zhao, X.; Xie, L. Adsorption Properties of Hydrocarbons (n-Decane, Methyl Cyclohexane and Toluene) on Clay Minerals: An Experimental Study. *Energies* **2017**, *10*, 1586. [CrossRef]
40. Quiroz-Estrada, K.; Hernández-Espinosa, M.; Rojas, F.; Portillo, R.; Rubio, E.; López, L. N_2 and CO_2 adsorption by soils with high kaolinite content from San Juan Amecac, Puebla, México. *Minerals* **2016**, *6*, 73. [CrossRef]
41. Dey, S.C.; Al-Amin, M.; Rashid, T.U.; Ashaduzzaman, M.; Shamsuddin, S.M. pH Induced Fabrication of Kaolinite-Chitosan Biocomposite. *Int. Lett. Chem. Phys. Astron.* **2016**, *68*, 1–9. [CrossRef]
42. Wang, L.; Zhang, J.; Zhao, R.; Li, C.; Li, Y.; Zhang, C. Adsorption of basic dyes on activated carbon prepared from Polygonum orientale Linn: Equilibrium, kinetic and thermodynamic studies. *Desalination* **2010**, *254*, 68–74. [CrossRef]
43. Dey, S.C.; Al-Amin, M.; Rashid, T.U.; Sultan, M.Z.; Ashaduzzaman, M.; Sarker, M.; Shamsuddin, S.M. Preparation, characterization and performance evaluation of chitosan as an adsorbent for remazol red. *Int. J. Latest Res. Eng. Technol.* **2016**, *2*, 52–62.

44. Ngah, W.S.W.; Ariff, N.F.M.; Hanafiah, M.A.K.M. Preparation, characterization, and environmental application of crosslinked chitosan-coated bentonite for tartrazine adsorption from aqueous solutions. *Water Air Soil Pollut.* **2010**, *206*, 225–236. [CrossRef]
45. Chen, D.; Chen, J.; Luan, X.; Ji, H.; Xia, Z. Characterization of anion–cationic surfactants modified montmorillonite and its application for the removal of methyl orange. *Chem. Eng. J.* **2011**, *171*, 1150–1158. [CrossRef]
46. Zaker, Y.; Hossain, M.A.; Islam, T.S.A. Adsorption kinetics of methylene blue onto clay fractionated from Bijoypur soil. *Bangladesh Res. J. Chem. Sci.* **2013**, *3*, 65–72.
47. Karima, B.; Mossab, B.L.; A-Hassen, M. Removal of methylene blue from aqueous solutions using an acid activated Algerian bentonite: Equilibrium and kinetic studies. In Proceedings of the International Renewable Energy Congress, Sousse, Tunisia, 5–7 November 2010; pp. 360–367.
48. Ghribi, A.; Bagane, M.; Chlendi, M. Sorptive removal of congo red from aqueous solutions using raw clay: Batch and dynamic studies. *Int. J. Innov. Environ. Stud. Res.* **2014**, *2*, 45–56.
49. Dunn, N.J.; Humphries, W.H., IV; Offenbacher, A.R.; King, T.L.; Gray, J.A. pH-dependent cis→trans isomerization rates for azobenzene dyes in aqueous solution. *J. Phys. Chem. A* **2009**, *113*, 13144–13151. [CrossRef]
50. Ara, N.J.; Abu Hasan, M.; Rahman, M.A.; Salam, M.A.; Salam, A.; Alam, A.S. Removal of Remazol Red from Textile Waste Water Using Treated Sawdust—An Effective Way of Effluent Treatment. *Pharm. J.* **2013**, *16*, 93–98. [CrossRef]



© 2019 by the authors. Licensee MDPI, Basel, Switzerland. This article is an open access article distributed under the terms and conditions of the Creative Commons Attribution (CC BY) license (http://creativecommons.org/licenses/by/4.0/).